Ibn Al-Haitham Journal for Pure and Applied Sciences
Journal homepage: jih.uobaghdad.edu.iq
PISSN: 1609-4042, EISSN: 2521-3407
IHJPAS. 2025, 38(2)

A Comprehensive Synthesis and Characterization via the Chemical Sol-Gel Method

Firas Salim Abed[1*] and Lamia K. Abbas[2]
[1,2]Department of Physics, College of Science, University of Baghdad, Baghdad, Iraq.
*Corresponding Author.

Received: 17 April 2024 Accepted: 2 September 2024 Published :20 April 2025
doi.org/10.30526/38.2.3979

Abstract

This research presents a synthesis approach for BSCCO superconductor with barium (Ba) substitution, involving a minor substitution at a fixed ratio of lead (Pb) and europium (Eu) through the chemical sol-gel method. The systematic exploration involves incorporating 0.1 of Eu instead of Bi into the BSCCO matrix to comprehend its impact on superconducting properties and the feasibility of producing superconducting material using the sol-gel route. Superconductor samples denoted as $Bi_{1.6}Pb_{0.3}Eu_{0.1}Sr_{2-y}Ba_yCa_2Cu_3O_{10+\delta}$, where y varies from 0.0 to 0.3, were prepared. The investigation focused on understanding the effect of partially substituting Ba for Sr on superconducting properties. Transmitted electron microscopy (TEM) results revealed the creation of nanoparticles with an average diameter of 104.7 nm using the sol-gel technique. X-ray diffraction (XRD) analysis exhibited mainly the high-Tc phase (2223) compared to the low phase (2212) and a higher a/c ratio was observed at y=0.1. Electrical resistivity measurements demonstrated an improvement in critical temperature (Tc), reaching 113 K, and an increase in oxygen content at the same ratio. This comprehensive investigation explores the influence of Ba substitution on the structural and superconducting properties of the BSCCO system prepared by the sol-gel technique for further exploration and optimization of these HTS for specific applications.

Keywords: BSCCO Superconductor, Sol-gel, High-temperature phase, XRD, TEM.

1. Introduction

Unconventional superconductivity in cup rate compounds (which include copper oxide layers) remains a focal point of continuing research, as evidenced by numerous studies (1). The exact mechanism of high-temperature superconductivity remains an active area of research and is not fully understood (2). The role of the layered structure and the interactions between the layers, particularly in materials containing CuO_2 planes, is a significant focus of the investigation (3). The specific arrangement of the CuO_2 planes and the interactions between them play a crucial role (4). Electrons move through these layers, and the interaction between adjacent layers is believed to be essential for the emergence of superconductivity (5). Superconducting behavior is thought to arise from the interaction between the electrons and the crystal lattice (6). Specifically when the temperature is lowered below a critical temperature

(Tc) (7), consequently, it is assumed that the critical temperature (Tc) of these materials can be manipulated by altering the electronic configuration of the CuO_2 planes, typically achieved through doping, thereby influencing the oxygen content within the compound (8). This way of research holds promise for the development of high-temperature superconductors with tailored properties. One of the most prominent materials in this field, bismuth-based superconductors, has received significant attention due to its high critical temperatures, which hold promise for applications in different fields such as magnetic resonance imaging (9, 10). The pseudo-tetragonal Bi-2223 unit cell is the fundamental structure of a high-temperature BSCCO system. However, obtaining a high-Tc (2223) single phase remains challenging. Nevertheless, it remains imperative to explore strategies to maximize the proportion of the (2223) phase within the material to elevate the critical temperature (11,12). Recent research suggests that partially melting Pb-doped materials and substituting Pb for Bi can significantly accelerate phase formation kinetics and enhance the yield of the Bi-2223 phase (13,14). Additionally, the superconducting behavior can be further optimized by double doping with additional elements (15). Achieving a homogeneous distribution of constituent parts within the sample is crucial for effective doping. Solid-state thermochemical processes stand out as the primary technique for fabricating ceramic superconductors (16), while alternative methods such as sol-gel procedures offer alternative routes to achieving a homogeneous mixture (17,18). The objective of this study is to investigate the correlation between the synthesis of Ba-substituted BSCCO using the sol-gel technique and their performance, suggesting a pathway for further advancements in high-temperature superconductors (19). The characterization of the synthesized samples involves an examination of their structural, morphological, and superconducting properties (20). Through the variation of the substitution factor and the application of advanced characterization techniques (21). This study offers insights into doping-induced changes in the crystal structure and superconducting transition temperatures (22).

2. Materials and Methods

Chemical sol-gel was employed to prepare Ba-modified BSCCO superconductor samples with Eu and Pb presence with the general formula $Bi_{1.6}Pb_{0.3}Eu_{0.1}Sr_{2-y}Ba_yCa_2Cu_3O_{10+\delta}$ at different values of y of 0, 0.1, 0.2, and 0.3. A set of raw materials of $Bi(NO_3)_2 \cdot 5H_2O$, $Eu(NO_3)_2$ $Pb(NO_3)_2$, $Sr(NO_3)_2$, $Ba(NO_3)_2$, $Ca(NO_3)_2 \cdot 4H_2O$, and $Cu(NO_3)_2 \cdot 3H_2O$, were used in their specified molar ratios. Ethylenediaminetetraacetic acid (EDTA) was utilized as a complexing agent, while urea served as a fuel at 0.7 molar ratios. Ethylene glycol (EG) was used as a binding agent with a cationic component of 3. The solvent system comprised nitric acid and distilled water. The synthesis procedure was initiated by introducing the nitrite salts dissolved into a specific volume of distilled water, followed by the addition of nitric acid. Each component's weight was according to its molar content in the samples. The resulting mixture was stirred at 45°C, and ethylene glycol was dissolved in a specific volume of distilled water, which was then combined with ethylenediaminetetraacetic acid (EDTA) to induce precipitation. Ammonium hydroxide (NH_3OH) was added to the primary liquid at 60°C until a pH of 7 was achieved, preventing precipitation and transforming the solution into a gel. This process was iterated for subsequent samples, and the resulting gel was further treated with the addition of urea. The gel underwent drying on a hot plate with gradual heating from 60 to 250°C in air, yielding a black-gray powder over 72 hours. A calcination procedure lasting six hours at 800° C was employed to eliminate residual nitrates, resulting in the formation of the final black BSCCO powder. This powder was homogenized using a gate mortar for half an hour. Then, pellets were fashioned from the powder samples using a hydraulic piston at 10-ton pressure. The pellets underwent a sintering process at 850°C for 48 hours, making them ready for subsequent characterization. The prepared samples were examined using X-ray diffraction analysis (SHIMADZU) to study structural properties such as the percentage of the high-temperature superconducting (HTS) phase and lattice parameters. The nano superconductors created were investigated using transmission electron microscopy (TEM) (Lasertec Corporation). Electric characterization was carried out using the four-probe method with the assistance of liquid nitrogen and a thermocouple. The critical temperature was determined by connecting electrodes to a Keithley instrument.

3. Results and Discussion

Figure 1 presents the x-ray diffraction patterns for $Bi_{1.6}Pb_{0.3}Eu_{0.1}Sr_{2-y}Ba_yCa_2Cu_3O_{10+\delta}$ samples, showing the impact of varying y factors. The diffraction patterns reveal a dual presence of both 2223 and 2212 phases within the samples. The percentage of the high-temperature superconductor phase 2223 changes with the partial substitution of Ba for Sr, as detected through diffraction peak intensities associated with the two phases. It's worth noting that in the diffraction patterns, there are weak diffraction peaks corresponding to an unidentified phase, indicating the possible presence of additional crystalline structures or phases.

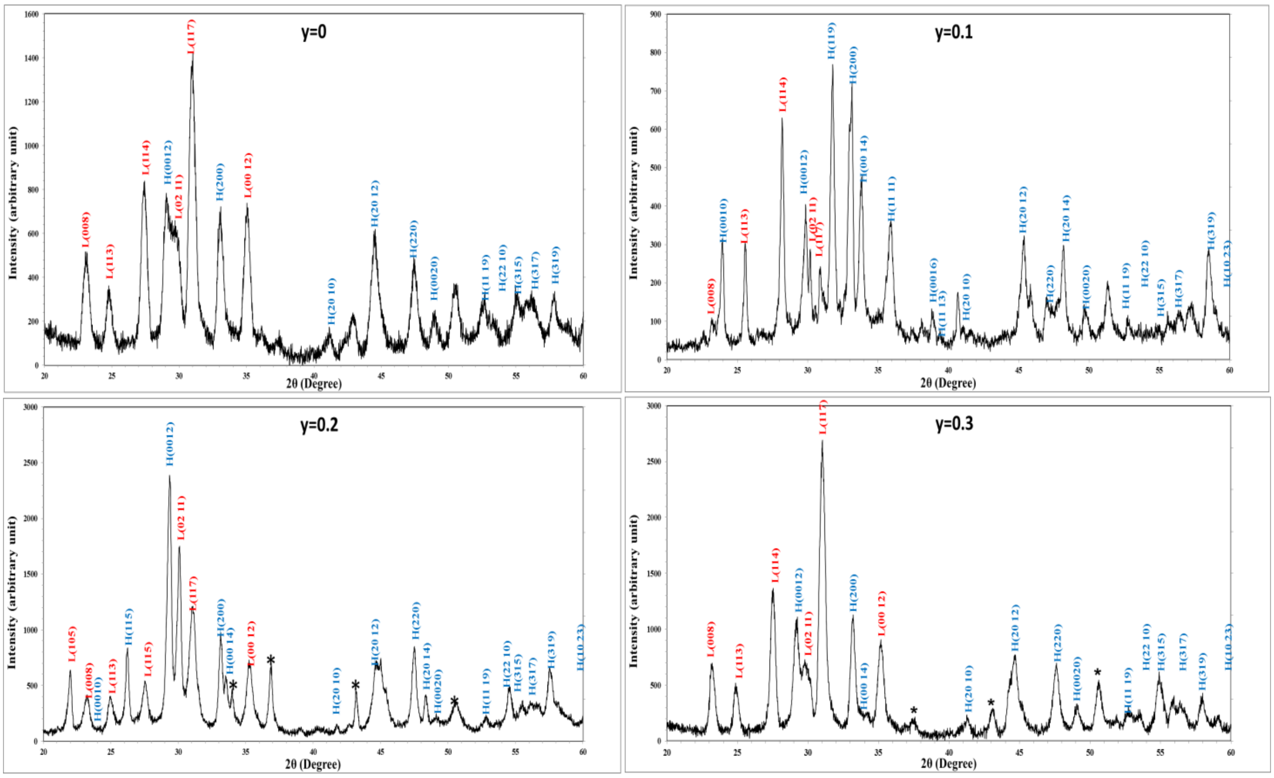

Figure 1. XRD patterns of $Bi_{1.6}Pb_{0.3}Eu_{0.1}Sr_{2-y}Ba_yCa_2Cu_3O_{10+\delta}$ at different values of y.

The investigation showed a peak HTS percentage of 75.99% for the 2232 phase at an optimal substitution factor of y=0.1. The certain dopant ratio may introduce necessary changes in the electronic structure of the material, promoting superconductivity. This can include enhancing the density of charge carriers by adding additional electron carriers, modifying the Fermi surface, or affecting the electron-phonon coupling, all of which contribute to an increase in the critical temperature (T_c) for superconductivity by facilitating electron movement without resistance. However, a subsequent increase in Ba substitution resulted in a decline in the HTS percentage. High substitution ratios can introduce disorder into the crystal structure, disrupting the coherence of the superconducting state. This disorder can impede the formation and movement of Cooper pairs, leading to a reduction in superconductivity, as discussed in a previous study (15). The higher Ba content leads to increased cuprite vacancies, causing enhanced scattering of super electrons within the crystalline structure (23). The diffraction peak positions observed in the samples exhibit slight variations with varying Ba content. The lattice constants were determined within the orthorhombic system by analyzing the diffraction peak positions. The variations in these lattice parameters concerning Ba content are graphically represented in **Figure 2**. For the sample with y=0 (no Ba substitution), the lattice parameters were found to be a=5.5203 Å, b=5.3183 Å, and c=36.7183 Å, closely resembling the values associated with the Bi-2201 phase. The heat treatment process induced reactions between the precursor and the added oxide, leading to variations in the lattice parameters. This can be attributed to the variance in ion diameter between the Ba dopant and the substituted ions of Sr, contributing to alterations in lattice constants and induced effects on other properties (24). **Table 1** provides a detailed account of the variations in lattice parameters (a, b, and c) with different Ba content. Moreover, Table 1 includes calculations of the c/a ratio and unit cell density (ρ) based on these lattice parameters (25), providing supplementary insights into the structural modifications brought about by Ba substitution. The recorded variations in lattice parameters and associated ratios reveal a notable peak in the c/a ratio at y=0.1, reaching 6.6649. This aligns with the higher observed HTS% at the same substitution ratio. This correlation underscores the significance of Ba substitution in influencing both the structural aspects and superconducting characteristics of the material (26).

Table 1. XRD parameters of $Bi_{1.6}Pb_{0.3}Eu_{0.1}Sr_{2-y}Ba_yCa_2Cu_3O_{10+\delta}$ at different values of y.

y	a (Å)	b (Å)	c (Å)	V (Å^3)	c/a	w (g/mole)	ρ_m (g/cm^3)	HTS %
0	5.5203	5.3183	36.7183	1078.004	6.6515	1017.752	6.2700	57.08%
0.1	5.4147	5.3105	36.0884	1037.711	6.6649	1022.723	6.5453	75.99%
0.2	5.5349	5.2927	36.4884	1068.895	6.5925	1027.694	6.3852	62.47%
0.3	5.5012	5.3023	36.6131	1067.979	6.6555	1032.665	6.4216	47.34%

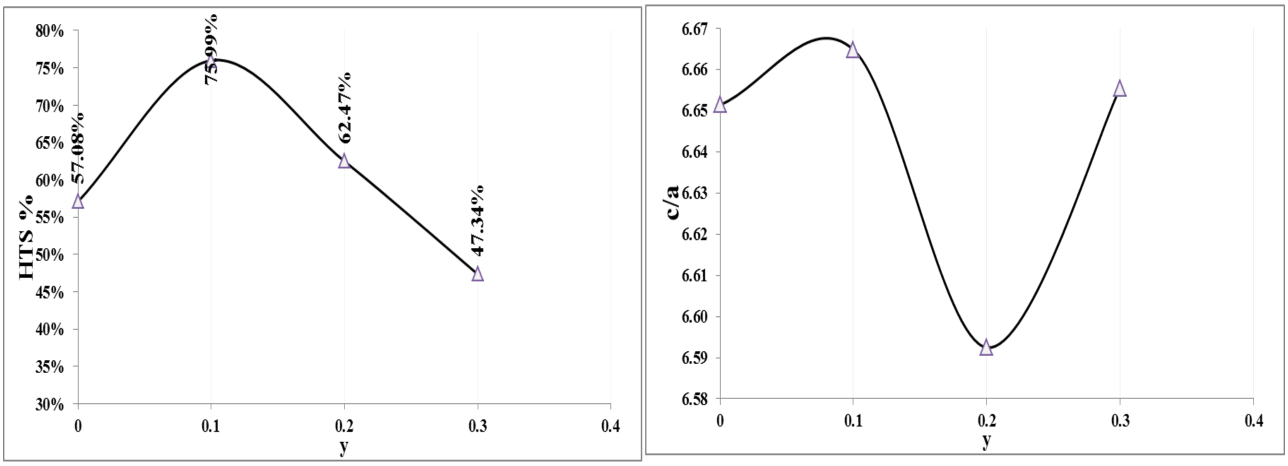

Figure 2. Variation of HTS, and c/a with y of $Bi_{1.6}Pb_{0.3}Eu_{0.1}Sr_{2-y}Ba_yCa_2Cu_3O_{10+\delta}$.

Figure 3 displays a Transmission Electron Microscopy (TEM) image of the $Bi_{1.6}Pb_{0.3}Eu_{0.1}Sr_2Ca_2Cu_3O_{10+\delta}$, accompanied by a histogram illustrating the particle diameter next to the image. The TEM image reveals the successful preparation of nanoparticles by the sol-gel technique, exhibiting nearly spherical shapes ranging in diameter from 50 to 250 nm. The particle size exhibits a uniform distribution, with an average diameter of 104.7 nm.

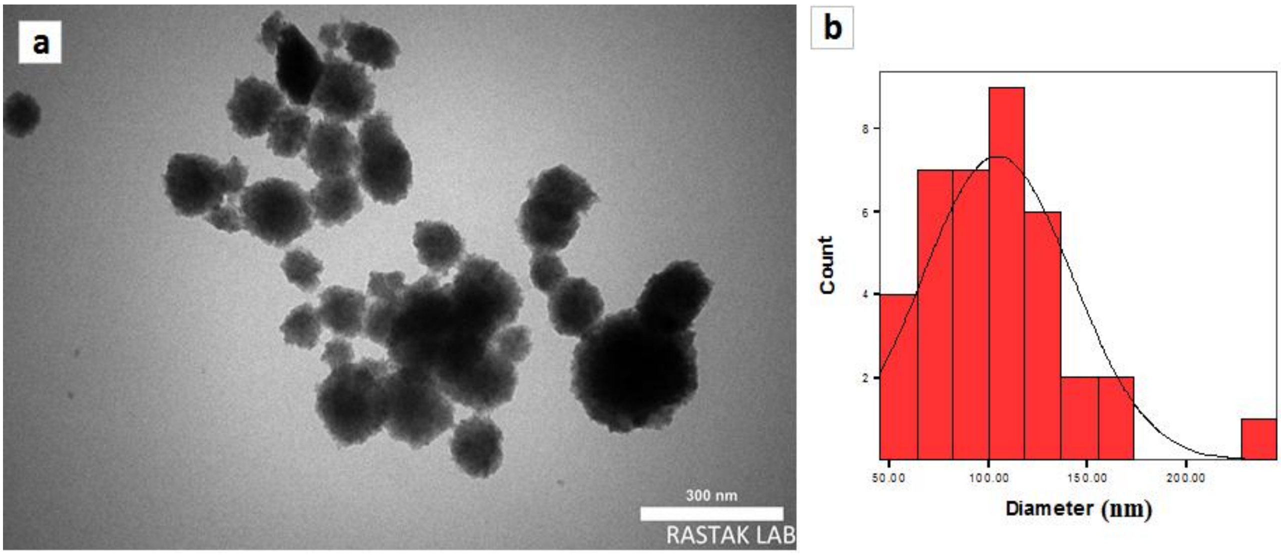

Figure 3. TEM image (a) and particle size distribution (b) of $Bi_{1.6}Pb_{0.3}Eu_{0.1}Sr_2Ca_2Cu_3O_{10+\delta}$ prepared by Sol-gel.

Figure 4 displays the EDS analysis for the $Bi_{1.6}Pb_{0.3}Eu_{0.1}Sr_2Ca_2Cu_3O_{10+\delta}$ samples prepared at different y values. The patterns show emission peaks corresponding to each atom.

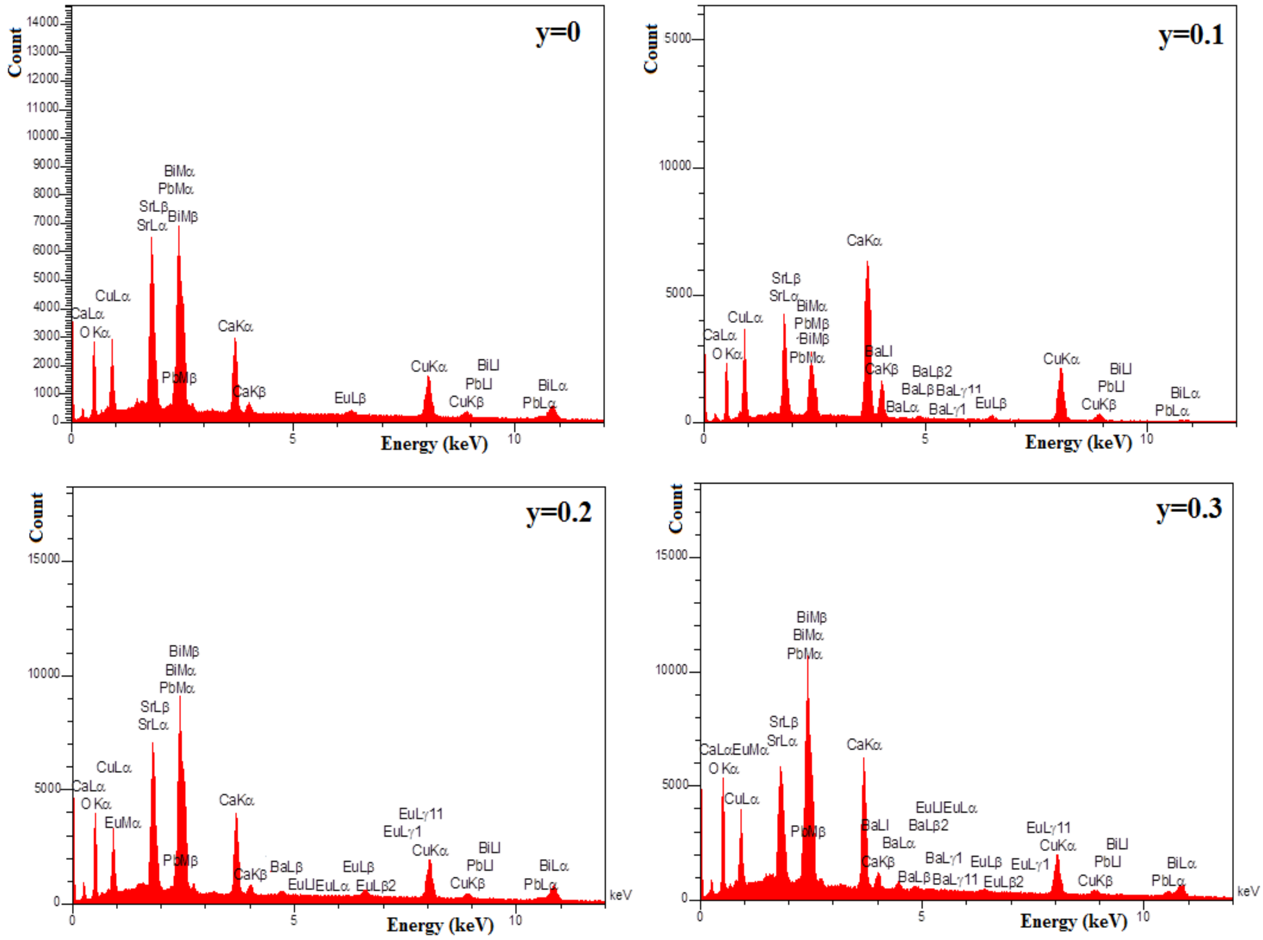

Figure 4. EDS spectra of $Bi_{1.6}Pb_{0.3}Eu_{0.1}Sr_{2-y}Ba_yCa_2Cu_3O_{10+\delta}$ at different values of y.

Table 2 lists the atomic ratio for each element in the four samples and the measured atomic ratio corresponding to all atoms within the samples of 19 atoms, compared with the stoichiometric ratios of each sample as listed in the general formula of $Bi_{1.6}Pb_{0.3}Eu_{0.1}Sr_2Ca_2Cu_3O_{10+\delta}$. The excess oxygen content in superconductors, beyond its stoichiometric ratio (δ), plays a crucial role in determining superconducting properties. In a pure BSCCO system, the excess greater than 10 arises from transferred electrons from Cu to the BiO layer, leading to the generation of holes on Cu and electrons on Bi. The changes in the valence state of Bi induced by the surplus oxygen result in alterations in hole carriers within the $Cu–O_2$ planes. Consequently, it is anticipated that the predominant excess of oxygen will be situated in the $Cu–O_2$ planes (27, 28). The oxygen ratio has its maximum ratio at y=0.1, followed by a reduction with further increases in y. This suggests a higher increase in oxygen beyond stoichiometric values for the 2223 structure, attributed to a more oxidized state of Ba^{2+} ions compared to Sr^{2+} ions (29).

Table 2. EDS analysis of $Bi_{1.6}Pb_{0.3}Eu_{0.1}Sr_{2-y}Ba_yCa_2Cu_3O_{10+\delta}$ at different values of y, the atomic ratio, and compared with the stoichiometric ratios.

y	Element	O	Ca	Cu	Sr	Eu	Ba	Pb	Bi
0	Atom%	53.8	16.39	11	11.61	0.7	-	0.72	5.78
	Measured ratio	10.22	3.11	2.09	2.21	0.13	-	0.14	1.10
	Stoch. ratio	10	3	2	2	0.1	-	0.3	1.7
0.1	Atom%	54.55	14.77	11	9.9	0.73	0.6	1	7.45
	Measured ratio	10.36	2.81	2.09	1.88	0.14	0.11	0.19	1.42
	Stoch. ratio	10	3	2	1.9	0.1	0.1	0.3	1.7
0.2	Atom%	54.16	15.33	9.9	9.5	0.83	1.02	1.52	7.74
	Measured ratio	10.29	2.91	1.88	1.81	0.16	0.19	0.29	1.47
	Stoch. ratio	10	3	1.9	1.8	0.1	0.2	0.3	1.7
0.3	Atom%	54.03	15.8	9.65	8.86	0.7	1.55	1.24	8.17
	Measured ratio	10.27	3.00	1.83	1.68	0.13	0.29	0.24	1.55
	Stoch. ratio	10	3	1.9	1.7	0.1	0.3	0.3	1.7

Figure 5 displays the electrical resistivity as a function of temperature for the $Bi_{1.6}Pb_{0.3}Eu_{0.1}Sr_2Ca_2Cu_3O_{10+\delta}$ samples at different y values. The rapid decline in resistivity as the temperature nears the critical temperature indicates the superconducting properties of the samples; the sudden decrease in resistance at T_c is caused by the creation of Cooper pairs of electrons, which can flow without any resistance below T_c. This is accompanied by the creation of an energy gap, which enables the dissipation-free flow of supercurrents (30). The critical temperature (T_c) values for each sample are detailed in Table 3. It is observed that the highest Tc value, reaching 113 K, is attained when y equals 0.1.

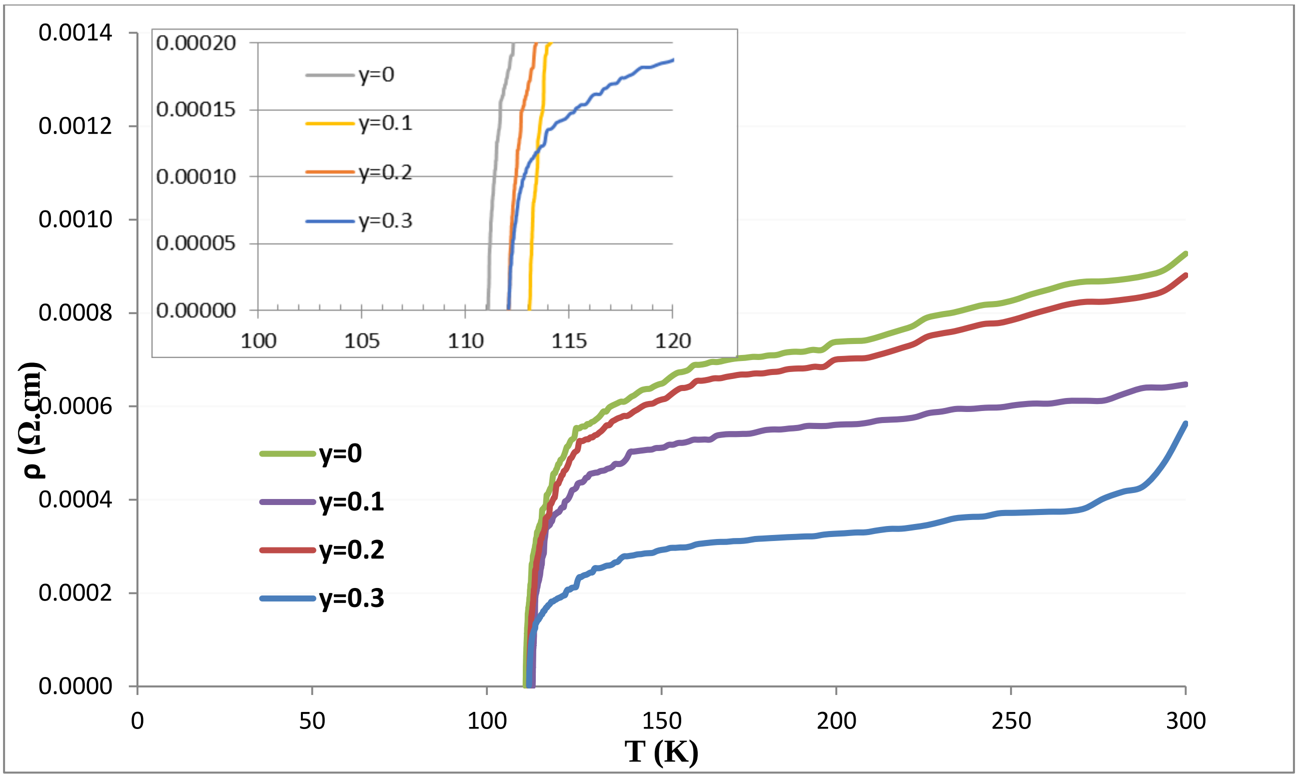

Figure 5. Variation of sample resistivity with a temperature of $Bi_{1.6}Pb_{0.3}Eu_{0.1}Sr_{2-y}Ba_yCa_2Cu_3O_{10+\delta}$ at different values of y.

Table 3. T_c values of $Bi_{1.6}Pb_{0.3}Eu_{0.1}Sr_{2-y}Ba_yCa_2Cu_3O_{10+\delta}$ at different values of y

	y=0	y=0.1	y=0.2	y=0.3
T_c (K)	111	113	112	112

4. Conclusion

Thin films of $Bi_{1.6}Pb_{0.3}Eu_{0.1}Sr_{2-y}Ba_yCa_2Cu_3O_{10+\delta}$ superconductor with (y=0.0, 0.1, 0.2, and 0.3) were obtained using the sol-gel method. XRD analysis reveals that deposited films exhibit polycrystalline multiphase formation with an orthorhombic phase. TEM provided thin films prepared in the nanoscale range. The value of the critical temperature obtained for different compositions demonstrated the dependence of T_c on the substitution of Ba ions, with the highest T_c value of 113 K achieved for y = 0.1, which shows an increasing behavior with the increase of Ba ratio, and these values for bulk specimens are higher than those for film specimens. We should mention that both the specimen's bulk and films showed a superconductor.

Acknowledgment

We would like to express our special thanks to Dr. Amal Kadhum Jasim and Mr. Mohanad A. Aswad for their support.

Conflict of Interest

There is no conflicts of interest.

Funding

Financial support in preparation for the publication is based on the corresponding author.

Ethical Clearance

Ethics of scientific research were carried out by the international conditions followed in dealing with laboratory animals and included animal health, husbandry and care for it, and providing appropriate conditions for it in terms of food, and appropriate methods were adopted in dealing with it when experimenting, and this is consistent with the instructions of the Iraqi Ministry of Health and Environment.

References

1. Stryczewska HD, Stępień MA, Boiko O. Plasma and Superconductivity for the Sustainable Development of Energy and the Environment. Energies (Basel). 2022;15(11):4092. https://doi.org/ 10.3390/en15114092
2. Hayden SM, Tranquada JM. Charge Correlations in Cuprate Superconductors. Annu Rev Condens Matter Phys. 2024;15(2). https://doi.org/10.1146/annurev-conmatphys-032922-094430
3. Laheeb A, Kareem AJ. Synthesis and study the Structural and electrical and mechanical properties of High Temperature Superconductor Tl0.5Pb0.5Ba2Can-1Cun-xNixO2n+3-Î´ Substituted with nickel oxide for n=3. Ibn Al-Haitham J Pure Appl Sci. 2018;31(3):26–32, https://doi.org/10. 30 723/ijp.v22i1.1212
4. Khaleel AK, Abbas LK. Synthesis and characterization of PVDF/PMMA/ZnO hybrid nanocomposite thin films for humidity sensor application. Optik (Stuttg). 2023;272:170288. https://doi.org/10.1088/140 2-4896/ad3868
5. O'Mahony SM. On the electron pairing mechanism of copper-oxide high-temperature superconductivity. Proceedings of the National Academy of Sciences. 2022;119(37). https://doi.org/10.1073/pnas.2207449119.
6. Haider HM, Wadi KM, Mahdi HA, Jasim KA, Shaban AH. Studying the partial substitution of barium with cadmium oxide and its effect on the electrical and structural properties of HgBa2Ca2 Cu3O 8+δ superconducting compound. AIP Conference Proceedings, American Institute of Physics Inc. 2019;12: 2311. https://doi.org/10.1063/1.5116960.
7. Afdlan MZ. The effect of Mg, Na, and Ce addition on the superconducting properties of Bi1.6Pb0.4Sr 2Ca2-xMxCu3Oy prepared sol-gel method. AIP Conference Proceedings, American Institute of Physics Inc. 2020;2333. https://doi.org/10.1063/5.0004299.
8. Agwamba EC. Superconductivity, quantum capacitance, and electronic structure investigation of transition metals (X = Y, Zr, Nb, Mo) encapsulated silicon nanoclusters (Si59X): Intuition from quantum and molecular mechanics. Mater Today Commun. 2023;37:107498, https://doi.org/10.1016/j. mtcomm.2023.107498.
9. Shimoyama J, Motoki T. Current Status of High-Temperature Superconducting Materials and their Various Applications. IEEJ Transactions on Electrical and Electronic Engineering. 2024;19(3):292–304, https://doi.org/10.1002/tee.23976.
10. Jassim AK, Salim AF. Dielectric Properties of Bi 2-x (Pb, Nd) x Sr 2 Ca 2 Cu 3 O 10+δ Superconducting System. Appl. Phys. 2019;23(2):23-34.
11. Mark AC. Structure and equation of state of Bi2Sr2Can-1Cun O2n+4+δ from x-ray diffraction to megabar pressures. Phys Rev Mater. 2023;7(2):34-55. https://doi.org/:10.1103/PhysRevMaterials. 7.064803.
12. Hussein BH, Mahdi SH, Makki SA, Al-Maiyaly BK. Synthesis and Study the Structure, electrical and optical properties of Bi 2-x Cd x Sr 2 Ca 2 Cu 3 O 10+ δ thin film Superconductors. Energy Procedia, Elsevier Ltd. 2019;12(3):100–110. https://doi.org/10.1016/j.egypro.2018.11.169.
13. Jassim AK, Abbas MM, Aljurani BA. Superconductivity properties and surface morphology of Bi-2223 compound doped with nano ago. 2nd International Conference For Engineering Sciences And Information Technology (Esit 2022): Esit2022 Conference Proceedings, AIP Publishing. 2024;220002. https://doi.org/10.1063/5.0183337.

14. Muhammed SA, Abbas NK. Synthesis and investigation of structural and optical properties of CdO: Ag nanoparticles of various concentrations. Baghdad Science Journal. 2023;20:2002–2011, https://doi.org/10.21123/bsj.2023.7292.
15. Sarun PM, Vinu S, Shabna R, Biju A, Syamaprasad U. Highly enhanced superconducting properties of Eu-doped (Bi,Pb)-2212. Mater Lett. 2008;62(7):2725–2728. https://doi.org/10.1016/j.matlet.2008. 01.026.
16. Antončík F, Jankovský O, Hlásek T, Bartůněk V. Nanosized Pinning Centers in the Rare Earth-Barium-Copper-Oxide Thin-Film Superconductors,. Nanomaterials. 2020;10(8):1429. https://doi.org/ 10.3390/nano10081429.
17. Zhao X. A process for the preparation of high-quality and uniform large-scale Bi2212 superconducting films via the sol-gel method. Journal of Materials Research and Technology. 2023;6:8337–8350, https://doi.org/10.1016/j.jmrt.2023.09.164.
18. Abbas MM, Jassim AK, Abdulridha R, Oboudi SF. Tailoring the superconducting properties for Bi1.7Pb0.3Sr2Ca2Cu3O10+d compound with addition of nano TiO2. 2nd International Conference For Engineering Sciences And Information Technology (Esit 2022): Esit2022 Conference Proceedings, AIP Publishing. 2024;220001. https://doi.org/10.1063/5.0183128.
19. Molodyk A, Larbalestier DC. The prospects of high-temperature superconductors. Science. 2023;380(6651):1220-2. https://doi.org/10.1126/science.abn2882.
20. Al Habeeb MQ, Oboudi S, Wenlong W, Julian S. Effect of Adding Ag Nanoparticles onto Magnetic and Structural Properties of BSCCO Superconducting Compound, Journal of Physics: Conference Series, IOP Publishing Ltd. 2021;23100. https://doi.org/10.1088/1742-6596/1829/1/012024.
21. Lojka M. Phase-stable segmentation of BSCCO high-temperature superconductor into micro-, meso-, and nano-size fractions. Journal of Materials Research and Technology. 2020;9(6):12071–12079, https://doi.org/10.1016/j.jmrt.2020.08.107.
22. Abdul-Hussein AA, Hasan N, Abdul-Hussein AM, Mohammed FQ. Synthesis of Bulk Superconductors Using the Sol-Gel Method. AIP Conference Proceedings, American Institute of Physics Inc. 2022. https://doi.org/10.1063/5.0108818.
23. Aljurani BA, Hermiz GY, Alias MF. Superconductivity Measurements of (Hg,Tl)-1223 Compound Prepared in Capsule. Iraqi Journal of Science. 2021;2934–2939, https://doi.org/10.24996/ijs.2021.62.9.9
24. Sam C, Mosbah M. Attaf S, Benbellat N. The Effect of Ba Doping on Sr site on Structural and Superconducting Properties of Bi2212 phase. Physica B: Physics of Condensed Matter. 2019;557:12–16. https://doi.org/10.1016/j.physb.2018.12.040
25. Aswad MA, Mutlak FA, Jabir MS, Abdulridha SK, Ahmed AF, Nayef UM. Laser assisted hydrothermal synthesis of magnetic ferrite nanoparticles for biomedical applications. Journal of Physics: Conference Series, IOP Publishing Ltd, Mar. 2021. https://doi.org/10.1088/1742-6596/1795/1/012030.
26. Wu C, Wang Y. Trilayer films of YBa2Cu3O7-x/LaAlO3/YBa2Cu3O7-x with superconducting properties prepared via sol-gel method. Coatings. 2020;10(7):12-23. https://doi.org/10.3390/en15114092 10.3390
27. Jassim AK, Abed FS. Enhancement of Tc by Substitution of (Pb And Nd) in Bismuth-Based High-Tc Superconductors Material. Journal of Non-Oxide Glasses. 2019;11(3):41–47.
28. Sedky A, Salah A. Comparative Study of the Effects of La-Substituted Ca in (Bi, Pb):2212 and (Bi, Pb):2223 Superconductors. J. Electron Mater. 2022;51(6):3042–3058. https://doi.org/10.1007/s11664-022-09476-z.
29. Onrubia-Calvo JA, Pereda-Ayo B, Cabrejas I, De-la-torre U, González-velasco JR. Ba-doped vs. Sr-doped $LaCoO_3$ perovskites as base catalyst in diesel exhaust purification. Mol Catal. .2020;488. https//doi.org:10.1016 /j.mcat.2020.110913
30. Tuama MJ, Abbas LK. Superconducting properties of Bi2-xPb0.3WxSr2Ca2Cu3O10+δ compounds. Iraqi J Sci.2021;62(2):490–495, http://doi.org/10. 24996/ijs.2021.62.2.15.2021